Role of surface wind and vegetation cover in multi-decadal variations of dust emission in the Sahara and Sahel

Dongchul Kim[1,2], Mian Chin[2], Lorraine A. Remer[3], Thomas Diehl[1,2,6], Huisheng Bian[2,3], Hongbin Yu[2,4], Molly E. Brown[2,4], William R. Stockwell[5]

[1]Universities Space Research Association, Columbia, Maryland, USA

[2]NASA Goddard Space Flight Center, Greenbelt, Maryland, USA

[3]JCET/UMBC, Baltimore County, Baltimore, Maryland, USA

[4]University of Maryland College Park, College Park, Maryland, USA

[5]Howard University, Washington D.C., USA

[6]European Commission, Joint Research Center, Ispra, Italy

Abstract

North Africa, the world's largest dust source, is non-uniform, consisting of a permanently arid region (Sahara), a semi-arid region (Sahel), and a relatively moist vegetated region (Savanna), each with very different rainfall patterns and surface conditions. This study aims to better understand the controlling factors that determine the variation of dust emission in North Africa over a 27-year period from 1982 to 2008, using observational data and model simulations. The results show that the model-derived Saharan dust emission is only correlated with the 10-m winds (W10m) obtained from reanalysis data, but the model-derived Sahel dust emission is correlated with both W10m and the Normalized Difference Vegetation Index (NDVI) that is obtained from satellite. While the Saharan dust accounts for 82 % of the continental North Africa dust emission (1340-1570 Tg year^{-1}) in the 27-year average, the Sahel accounts for 17 % with a larger

seasonal and inter-annual variation (230-380 Tg $year^{-1}$), contributing about a quarter of the transatlantic dust transported to the northern part of South America. The decreasing dust emission trend over the 27-year period is highly correlated with W10m over the Sahara (R=0.92). Over the Sahel, the dust emission is correlated with W10m (R=0.69) but is also anti-correlated with the trend of NDVI (R=-0.65). W10m is decreasing over both the Sahara and the Sahel between 1982 and 2008, and the trends are correlated (R=0.53), suggesting that Saharan/Sahelian surface winds are a coupled system, driving the inter-annual variation of dust emission.

1. Introduction

Dust plays an important role in global climate by interacting with solar and terrestrial radiation, altering cloud amount and radiative properties (Haywood et al., 2003; Forster et al., 2007; Evan et al., 2008; Kim et al., 2010). Dust is also important to biogeochemical cycles by fertilizing land and ocean and modulating carbon uptake (Jickells et al., 2005; Maher et al., 2010; Yu et al., 2015a). North Africa is the world's largest dust source accounting for about one half of the global dust mass loading in the atmosphere (Kinne et al., 2006; Chin et al., 2009), and its impact can go well beyond the source region extending to hemispheric or even global scales (Carlson and Prospero, 1972; Kaufman et al., 2005; Prospero, 2014; Yu et al., 2015b). Mineral dust is also an air pollutant that causes premature deaths by cardiopulmonary disease and lung cancer (Giannadaki et al., 2014).

North Africa is known to be the largest dust source area in the world, but the dust sources are not homogeneously distributed (Ginoux et al., 2001, 2012; Formenti et al.,

2011). For example, the Köppen-Geiger climate classifies North Africa into three regions with the Sahara desert in the north, the Savanna in the south, and the Sahel, a semi-arid transition zone, between the two (Kottek et al., 2006). Although the Saharan desert is considered to be the major dust source in North Africa, a number of previous observational and modeling studies have found that the dust sources in Sahel plays an important role in the North African climate system (Charney, 1975; Tegen et al., 2004; Yoshioka et al., 2007; Foltz and McPhaden, 2008; Mahowald et al., 2010; Klose et al., 2010; Cowie et al., 2013).

Dust emission from bare soil is mainly driven by surface wind interacting with dry soil particles. When the surface is vegetated, the vegetation protects underlying soils and plays an important role in modulating the quantity of dust emitted. However, the relationship between wind and vegetation as well as their roles in dust emission is not fully understood. For example, there is a suggestion that decreasing surface wind speed since the 1980s in North Africa can be explained by increased vegetation that enhances surface roughness (Vautard et al., 2010; Bichet et al., 2012; Wang et al., 2012; Cowie et al., 2013). While some studies find that precipitation and vegetation together strongly constrain dust over the Sahel and other semi-arid source regions (e.g., Prospero and Lamb, 2003; Zender and Kwon, 2005; Cowie et al., 2013), others do not find a direct link between the dustiness of the Northern Atlantic and the land use or vegetation change over the source region (e.g., Ridley et al., 2014).

Because the Sahara is mostly bare, experiencing no significant seasonal or interannual variability in surface characteristics, we expect any variability in dust sources from this area will be due to meteorology, specifically surface wind speed, and not due to

changes in vegetation. If there is variability in dust source strength in North Africa linked to vegetation cover, that variability will be introduced by Sahel sources with their seasonal and interannual vegetative cover variability. That is why characterizing dust source processes in the Sahel is central towards better understanding the relative roles of meteorology and land surface processes in dust emissions for the Sahel and the North Africa. The goal of this study is to better understand the relationships between surface wind, rainfall, surface vegetation, dust emission, and dust loading over the Sahara and Sahel using wind and vegetation data sets and global dust model simulations in a multi-decadal time span from 1982 to 2008.

In this paper, we first define in Section 2 the sub-Saharan semi-arid region (i.e., the Sahel) using the satellite observations of Normalized Difference Vegetation Index (NDVI), and describe the NASA Goddard Chemistry Aerosol Radiation and Transport (GOCART) model used in this study. In Section 3.1 we compare modeled dust optical depth (DOD) with remotely sensed and in situ observations. In Section 3.2 we examine the long-term climatological mean seasonal relationships between surface conditions and meteorological parameters over the Sahara and Sahel. We then estimate the contribution of the Sahelian dust transport to the dust loading over the North Atlantic in Section 3.3, followed by a time-dependent analysis of model-derived dust emission with two independent observationally-based trends of surface wind and surface vegetation over the time span between 1982 and 2008 in Section 3.4. Discussion and summary are given in Sections 4 and 5, respectively.

2. Methods

2.1 Sahel area determined by the AVHRR NDVI

We have utilized the Normalized Difference Vegetation Index observed from the Advanced Very High Resolution Radiometer satellite (AVHRR-NDVI) to build a Sahel area map (Kim et al., 2013). The 8-km, half-monthly AVHRR NDVI composite data (version NDVIg) is from the NASA Global Inventory Monitoring and Modeling Systems (GIMMS) that spans the years August 1981 to December 2008 (Tucker et al., 2005; Brown et al., 2006; Anyamba et al., 2014). Our method for Sahel area determination relies on a condition that may characterize the behavior of NDVI in North Africa based on an analysis of the NDVI throughout the period of NDVIg availability (January 1982 to December 2008) to be consistent with the method developed in the previous study (i.e., Kim et al., 2013), even though a newer version (NDVI3g) has expanded to cover the present time (Pinzon and Tucker, 2014; Anyamba et al., 2014).

The Sahara and Sahel exhibit different values and variability of NDVI throughout the year. NDVI is always lower than 0.15 in the northern part of the domain and always greater than 0.2 in the southern part of the domain (Figure 1a and 1b). In the transition zone, the NDVI is below 0.15 during the dry season and it is greater than 0.20 during the wet season. Thus, we define the annual semi-arid transition zone, or the Sahel, as the area that complies with the following criteria:

$$NDVI_{min} < 0.15 \text{ and } NDVI_{max} > 0.20 \quad (1)$$

where $NDVI_{min}$ and $NDVI_{max}$ are the minimum and maximum monthly values of NDVI in a particular latitude-longitude grid point in a given year. We have applied these

conditions to the area for 10°N-20°N and 17°W-40°E (Figure 1c). The shape and location of the Sahel defined by equation (1) is quite similar to other studies using precipitation amount (e.g., Herrmann et al., 2005; Kottek et al., 2006; Anyamba et al., 2014). The semi-arid area defined here clearly excludes all permanent deserts from the Sahel similar to the precipitation based map (e.g., the Bodélé depression at 17°N,18°E). There is some year-to-year change in the southern Sahel border and in the total area of the semi-arid region, but the northern Sahel border is generally the same. A climatological semi-arid region calculated based on the AVHRR NDVI in this study, which can be considered as the general Sahel area, is shown in Figure 1d at 1° latitude × 1.25° longitude resolution. In the map, a grid point is determined as the Sahel when it satisfies the equation (1) for more than 5 years out of the 27-year data base. The blue area is identified as the semi-arid Sahel (3.6×10^6 km^2) and the red indicates the permanent Sahara desert (1.1×10^7 km^2).

2.2 GOCART model description and simulation setup

The Goddard Chemistry Aerosol Radiation and Transport (GOCART) model is used to simulate key tropospheric aerosols including sulfate, dust, black carbon, organic carbon, and sea-salt (Ginoux et al., 2001; Chin et al., 2002, 2009, 2014). The model is driven by the meteorological reanalysis data from the Modern-Era Reanalysis for Research and Applications (MERRA) (Rienecker et al., 2011) with the input of the meteorological fields from MERRA every 3 hours, which were linearly interpolated to the GOCART model dynamic time step (15 min, in this case). The model is run as an offline chemistry transport model with no feedback between dust and meteorology. We run the model simulation at a spatial resolution of 2° latitude × 2.5° longitude and 72

vertical layers up to 0.01 hPa. Aerosol advection is computed by a flux-form semi-Lagrangian method that is a second-order closure scheme for the boundary layer turbulent mixing, and the moist convection is based on the cloud mass flux fields (details given in our previous publications, e.g., Chin et al., 2002, 2009).

The dust emission parameterization in GOCART requires the 10-m wind speed, the threshold velocity of wind erosion, and the surface conditions (soil type, ground wetness, topographic depression, and surface bareness) (Ginoux et al., 2001). Dust emission flux E_p (μg m^{-2} s^{-1}) for a size group p is expressed as:

$$E_p = C \times S \times s_p \times W_{10m}{}^2 \times (W_{10\mathrm{m}} - W_t), \text{ if } W_{10\mathrm{m}} > W_t \quad (2)$$

where C is a dimensional factor (μg s^2 m^{-5}), S is the dust source function described below, s_p is the fraction of size group p within the soil (Tegen and Fung, 1994), W_{10m} is the 10m wind speed (m s^{-1}), and W_t is the threshold velocity of wind erosion as a function of dust density, particle diameter, and surface wetness to account for the bonding effect between water and particles (Ginoux et al., 2001, 2004). Two soil types considered for erosion are clay (particle radius less than 1 μm) and silt (particle radius greater than 1 μm and less then 10 μm). S is the dust source function or probability of dust uplifting with a value between 0 and 1. The dust source function S is a product of the degree of topographical depression (H) and surface bareness (B), where H is calculated from the elevation of the grid cell relative to the elevation of the surrounding areas (Ginoux et al., 2001), and B is defined as the fraction of the NDVI pixels in a model grid cell that are below a threshold value of 0.15 (Kim et al., 2013). Such defined surface bareness resolves the seasonal and inter-annual variation of the dust source function in semi-arid area based on the time-

dependent variation of NDVI (Kim et al., 2013). Dust particle size distribution is described by eight size bins in the size range from 0.1 to 10 μm in radius to take into account size-dependent physical and optical processes (Chin et al., 2009). GOCART explicitly calculates dust emission and deposition processes for 5 size bins in the range of 0.1 – 1.0 – 1.8 – 3.0 – 6.0 – 10.0 μm in diameter. The first mass size bin is further divided into 4 sub-size bins for optical property calculations (Tegen and Fung, 1994; Ginoux et al., 2001). The model does not include dust particles larger than 10 μm in diameter, because they are removed from the atmosphere quickly (lifetime only a few hours) to have small impact on transport and radiative effects (Tegen and Fung, 1994; Ginoux et al., 2001). Physical processes include boundary layer mixing, advection, convective transport, and dry and wet depositions. More complete description of the GOCART model and the dynamic dust source function can be found in previous publications (see Kim et al., 2013 and references therein).

We performed two sets of simulations using GOCART for the three-decadal period from 1982 to 2008 using the NDVIg data. First, in a base run dust is emitted from all global source regions including Sahara, Sahel, Middle East, Central and East Asia, and other source regions. In the second run dust emission is restricted to only the Sahel domain described in section 2.2 (see Figure 1d) in order to quantify the Sahel contributions. Our analysis in this study focuses on the domain covering North Africa and North Atlantic between 90°W-40°E and 0°-35°N.

2.3. Observations

We compare the model-simulated dust optical depth (DOD) with several observational data sets. Two satellite products for 2001-2007 are used: the Multiangle Imaging Spectroradiometer (MISR) (Kahn et al., 2005) and the Moderate Resolution Imaging Spectroradiometer (MODIS). The MODIS DOD over ocean is derived from the AOD (dark-target product, Remer et al., 2005; Levy et al., 2010) and fine-mode fraction (f) over ocean to empirically separate DOD from the anthropogenic and marine aerosols using representative values of fine mode fractions of marine, dust, and anthropogenic aerosols and marine aerosol optical depth (Kaufman et al., 2005; Yu et al., 2009). For MISR, the non-spherical AOD is assumed to be equivalent to the DOD (Guo et al., 2013). We also use the ground-based remote sensing data from the AErosol RObotic NETwork (AERONET, Holben et al., 1998); the coarse-mode AOD derived from AERONET direct sun measurements at the wavelength 550 nm is used as a proxy of DOD (Dubovik et al., 2000, 2002, and 2006; Eck et al., 2010). There are eight AERONET stations located in the study domain (Agoufou, Banizoumbou, Ouagadougou, Dahkla, Dakar, Cape Verde, La Parguera, and Surinam; see Figure 2 for a map of the locations). Note that the DOD from satellites and AERONET are derived based on the particle size or shape information with several assumptions, they should be considered as proxies of dust rather than the "true" DOD.

2.4 Modern-Era Reanalysis for Research and Applications (MERRA) products

Besides driving the GOCART model runs, MERRA reanalysis products of key meteorological fields pertinent to dust are used in our analysis. Specifically we call upon W10m and precipitation, for their determining roles in dust emission and removal. The

209 reanalysis system ingests data from a variety of sources including ground-based stations,
210 radiosondes and satellite products. The information content is then relaxed through a 4-
211 dimensional model grid to produce physically consistent fields of data that are easily
212 matched to gridded satellite data and other model output.

213 There have been attempts to validate Sahelian reanalysis products or test
214 consistency between different reanalysis data sets with mixed results. Cowie et al. (2013)
215 and Ridley et al. (2014) show consistency between different reanalysis systems' depiction
216 of the broad features of the W10m field. Specifically all surface wind products show a
217 downward trend during the time period of our interest. However, the same cannot be said
218 for the precipitation, which varies significantly between data sets based on the global
219 gauge-based NOAA Climate Prediction Center "Unified" (CPCU) precipitation product
220 (Reichle et al., 2011) and those based on the Global Precipitation Climatology Centre
221 (GPCC) system (Beck et al., 2005). The problem in North Africa is the sparse distribution
222 of surface stations and radiosondes and the high spatial variability of precipitation.
223 Unlike precipitation, surface winds are more strongly coupled to upper level winds, more
224 spatially coherent and easier to represent properly in the reanalysis system.

225 In the analysis presented below, we show both W10m and precipitation reanalysis
226 fields from MERRA. Because of the large uncertainty in the precipitation product,
227 especially its interannual variation and long-term trends, we use it mainly to show the
228 climatological seasonal variations averaged over the study time period (27 years).
229

230 3. Results

231 3.1. Comparisons of model results with satellite and AERONET data

Although dust emission is the major variable of interest, there is no known validation data for dust emission for the study area and period. The variable that we can compare with other measurements is the dust aerosol loading in the atmosphere, once the dust is airborne. Already the GOCART model aerosol loading has been extensively compared with various observations over global and regional scales, including our area of interest (Chin et al., 2007, 2014; Yu et al., 2009, 2015b; Kim et al., 2013). In this section we add to this growing body of GOCART validation by comparing the spatial and temporal variations of the modeled DOD with the satellite and ground observations averaged for 2001 to 2007 over the study domain. We show this comparison between the satellite retrievals and the model to assess the model's ability in representing the seasonal variation of DOD in the North Atlantic.

The dust optical depth from the model and observations are shown in Figure 2. The maximum DOD from the model (Figure 2c) is greater than 0.5 and is located over Western Africa near source regions. Modeled DOD values decrease westward from the source regions, over the Atlantic Ocean, as particles are removed by dry and wet deposition during transport by the prevailing easterlies. The oceanic averaged DOD from the model (0.06) is lower than that from the satellite observations of coarse mode AOD or non-spherical AOD (0.10-0.12). As shown in Figure 2a and 2b as well as in our previous study (Kim et al., 2014), the east-to-west gradient across the North Atlantic is much stronger in the model than in the satellite observations, and the latter agree better with the AERONET measurements. Because of the seasonal changes in winds and precipitation associated with movement of the Inter Tropical Convergence Zone (ITCZ), the dust center located at 10°N-20°N over the ocean during summer shifts further south to around

0°-15°N in winter, seen in both satellite retrievals and the model. The model and satellites also indicate that DOD over the ocean is higher in summer (0.08-0.16) than in winter (0.06-0.11). The model shows that the magnitudes of the peak DOD vary by locations and time over North Africa, with a peak over southern/central Sahel in winter but over western Sahara in summer.

Figure 3 shows the seasonality of the monthly mean DOD over land from GOCART (Figure 3a) and over ocean from GOCART and satellite retrievals (Figure 3b and 3c). Monthly mean model-calculated and satellite-derived DOD over the Eastern- and Western Atlantic Ocean, divided at 50°W, shows the seasonality of the dust loading as the dust is transported across the Atlantic. Although DOD from MODIS is larger than MISR by up to 0.05 in the western North Atlantic in spring, the two satellite data agree within their standard deviations over the Eastern Atlantic and their seasonal patterns are similar. The modeled DOD is about 0.01-0.05 lower than the satellite data over the eastern North Atlantic, but it is a factor of 2-5 too low over the western North Atlantic, most likely due to the strong removal processes in the model during transport, noted by a previous study (i.e., Kim et al., 2014). Nonetheless, the model captures the seasonal variations of DOD over both eastern and western North Atlantic, showing a maximum value in July. The GOCART-Sahel result is discussed in section 3.3.

The column dust optical depth (DOD) of the model is compared with coarse mode AOD (proxy of DOD) retrieved at the 6 AERONET sites over the Sahel for the period of 1999-2008 (Figure 4). DOD at the three inland AERONET sites (i.e., Banizoumbou, Ouagadougou, and Agoufou) shows similar seasonality with maxima in spring and summer (March-July) and minima in winter (November-February) with mean DOD

between 0.43 and 0.50. AERONET DOD at Cape Verde and Dakar (DOD = 0.35-0.41), which is located on the west coast, is lower than the inland sites and exhibits large intra-seasonal variations. At Dakar, the model captures the magnitude of AERONET coarse mode AOD but shows different seasonal variations (r = 0.01); interestingly, the total AOD calculated by the model agrees much better with the AERONET measured total AOD at Dakar (r=0.43, not shown), reflecting the uncertainties in approximating DOD with coarse mode AOD in Dakar. Overall, the scatter plots in Figure 4 indicate the degree of similarities between model calculated DOD and AERONET retrieved coarse model AOD at the 6 sites in Sahel, with mean bias between 0.91 and 1.66 and correlation coefficients between 0.01 and 0.84.

3.2. Seasonal variation of dust emission and controlling factors

In this section we examine the relationships of atmospheric and surface conditions with dust emission and dust mass loading over different sub-regions of North Africa. NDVI, rainfall, and W10m are used to represent atmospheric and land conditions. Dust related parameters are taken from the GOCART model including source function (S), bareness, dust emission, and dust column loading (LOAD). Climatological monthly values of these parameters are calculated during the time period from 1982 to 2008 for the Sahara and Sahel (Figure 5). Note that emission and loading in Figure 5b are normalized to their maximum values in North Africa of 1.22×10^{7} g km^{-2} mon^{-1} and 10.1 g km^{-2}, respectively. All variation noted in this section is seasonal variation based on long-term averages. Correlations in Table 1 refer to seasonal progressions and are each calculated from data sets with N = 12.

First, small rainfall amounts over the Sahara, a permanent desert with average rainfall less than 0.3 mm/day, result in low NDVI (~0.1) and high bareness (~0.9) throughout year (Figure 5a, left panel). S, which is a product of surface bareness and topographic depression, is almost constant throughout the year with a value around 0.25 (Figure 5a, left panel). In contrast, those variables (NDVI, S, bareness, and rainfall) exhibit much stronger seasonal variations in the Sahel (Figure 5a, right panel). The wet season in Sahel is between March and October with a peak rainfall of 3.3 mm day^{-1} in July. The dry season is ranging from November to February. The effect of the seasonal progression of the rainfall on the vegetation is clearly seen in the annual cycle of the NDVI in the Sahel. The NDVI is positively correlated with rainfall (R=0.61) (Table 1), with a peak in September (0.3) occurring about a month after the peak rainfall and a minimum in June (0.15) occurring just before the heavy rains (> 2 mm day^{-1}) begin. Consequently the bareness over the Sahel shows a seasonal variation that is opposite to the NDVI with a maximum in June (~0.7) and minimum in September (~0.4). S has the same seasonality as the bareness with a peak in June (~0.25) and a minimum value in September (~0.18). The 28 % reduction of S in September compared to June is caused by the seasonal variation of surface vegetation.

Climatological monthly averaged W10m from MERRA over the Sahara ranges between 4.2 and 4.5 m s^{-1}, with the spring season (March to May) slightly higher than the fall season (Figure 5b, left panel). Consequently dust emission is higher in spring than in fall. The 0.3 m s^{-1} differences in W10m cause about a 20% difference in dust emission due to the third power relationship between wind speed and dust emission (see equation 2). Indeed we see how the emissions follow the same seasonal pattern as W10m. Because

of the dryness and little vegetation cover, the change in winds over the Sahara provides the best explanation for the seasonal cycle of emission. Over the Sahel (Figure 5b, right panel), W10m shows a much stronger seasonal variation, ranging between 3 m s^{-1} in September and 5 m s^{-1} during winter. The W10m seasonal variation over the Sahel is anti-correlated with NDVI (R=-0.64) that peaks in September. The strong anti-correlation between W10m and rainfall (R=-0.82) indicates that the wind speed during the rainy season is weaker than the dry season. The dust emission shows the same seasonal variation as W10m with a maximum in winter and a minimum in August-September. The Sahel emission flux per unit area is 62% of the Sahara because of less bareness (average of 0.51 compared to 0.88 for the Sahara), weaker W10m (average of 4.10 m s^{-1} compared to 4.47 m s^{-1} over Sahara), and lower S (average of 0.20 compared to 0.25 for the Sahara). The total emission from the Sahel (308 Tg $year^{-1}$) is only about 21 % of the Sahara (1476 Tg $year^{-1}$). This is because of the lower emission rates and smaller area of the Sahel (3.6×10^6 km^2) compared to the Sahara (1.1×10^7 km^2).

Strong anti-correlations are found between NDVI and dust emission (R=-0.87) and between NDVI and loading (R=-0.63) over the Sahel (Table 1). The strongest correlation coefficients (R>0.9) are found between W10m and emission over both the Sahara and the Sahel (Table 1). On the other hand, no significant correlation between W10m and dust loading (mass per unit area) is found in either region (R<0.1). In the Sahara, dust loading shows a peak season in spring and summer (April to August) and minimum in winter (December and January). In the Sahel, the primary peak dust loading occurs in April to June, similar to the Sahara, with the column loading per unit area over the Sahel greater than over the Sahara. The larger loading over the Sahel than the Sahara

suggests the dominant source of dust loading over the Sahel is actually transported dust from the North. Shao et al. (2010) estimate that 50% of Saharan dust emissions are transported to the south. The remaining half are transported to West (30%), North (15%), and East (5%). Klose et al. (2010) agree with this assessment and show that the synoptic situation that favors northeasterly winds that transport dust from the Sahara to the Sahel and beyond to over the Gulf of Guinea is most frequently seen in the Spring.

Overall, the variation of magnitude and seasonality of dust emission predominantly responds to the change of wind speed over both the Sahara and Sahel. Secondly, the correlation coefficient analysis suggests that over the Sahel, unlike the Sahara, NDVI is also tied to dust emission for seasonal climatology (R=-0.87).

3.3. Contributions of the Sahel dust source to North Africa and Northern Atlantic dust loading

In this section we estimate the 27-year averaged relative contribution of the Sahel dust emission to North Africa and Northern Atlantic dust loading using the GOCART model simulations from the base and Sahel source runs (described in Section 2.2). The Sahel contributes about 17 % (308 Tg $year^{-1}$) of the North African dust emission (1805 Tg $year^{-1}$) ranging from 7 % in September to 22 % in January-February (Figure 6). Saharan dust accounts for 82 % (1497 Tg $year^{-1}$) of the North African dust (79 % in winter and 86 % in summer). The Sahara and Sahel together account for 99% of the North African dust emission while a miniscule fraction of dust is emitted from the south of the Sahel. Unlike the relatively constant wind field throughout the year over the Sahara (i.e., Figure 5b, left panel), the strong seasonal variation of wind and perhaps vegetation

over the Sahel (i.e., Figure 5b, right panel) results in a maximum emission in January-March (33 Tg mon^{-1}), which is nearly a factor of four over the minimum dust emission season of August-September (9 Tg mon^{-1}) in Sahel.

Using the two GOCART model runs (base and Sahel source only), we can quantify the fraction of the Sahel sources that contribute to the dust loading in the study domain. In the base run that includes all global sources of dust, DOD is highest over North Africa, decreasing over the Northern Atlantic Ocean (Figure 7a). In the run with only Sahel sources, the magnitude of the DOD is less and the distribution shifts to the south (Figure 7b). The distribution of DOD fraction contributed by Sahel sources is shown in Figure 7c. The fraction of DOD contributed by the Sahel never exceeds 50 % any place in the domain. Over the Sahel itself, only 40 % of the DOD in winter and 30 % of the DOD in summer originates from dust sources in the Sahel (Figure 7c). Simulations show that most of the dust from Sahel sources is transported toward the southwest throughout the year. This result implies that the Sahel is an important source of dust over the tropical regions during the winter season, accounting for 30~40 % of the DOD there. The longitudinal gradient of the Sahel DOD fraction indicates the non-linear contributions of emission, deposition, and transport between source and long-range transport. Also there is a strong latitudinal contrast of the Sahel DOD fraction centered at 20°N, i.e., the Sahel DOD fraction is less than 15 % to the north of 20°N but between 15% (summer) and 40% (winter) to the south of 20°N. These simulations are consistent with observations (Prospero et al., 2014). The model suggests that the Sahel dust contributes about a quarter (20-25 %) of the dust found over the northern part of South America.

393 The model simulations show that the DOD seasonality of the Sahel dust does not
394 drive the seasonality of the dust found over the total domain, which has a peak in spring-
395 summer and minimum in winter (Figure 3a). Instead the DOD seasonality of the Sahel
396 dust peaks between December and May and exhibits a minimum in August and
397 September.
398
399 3.4. Inter-annual variability and long-term trends
400 Up to this point we have investigated dust emission and dust loading for a
401 climatological annual cycle. Now we further examine the Sahara and Sahel dust and
402 environmental controlling parameters for inter-annual variations and long-term trends.
403 Anomalies of annual W10m and emission are calculated for the Sahara and the Sahel
404 from 1982 to 2008 (Figure 8a and 8b). Since W10m is the driving force for dust emission
405 in the GOCART model (Eq. 2), a strong positive correlation between them is expected.
406 Indeed, over the Sahara the correlation coefficient between W10m and emission is high
407 (R=0.92). The annual mean and standard deviation of emission and W10m are 11.5±0.42
408 (g m^{-2} mon^{-1}) and 4.47±0.05 (m s^{-1}), respectively, over the 27-year period. There is a
409 steady decreasing trend in both variables from the 1980s to the mid-2000s. W10m
410 decreases at a rate of -0.0042 m s^{-1} (0.09%) per year, while Saharan emissions decrease at
411 a rate of -0.026 g m^{-2} mon^{-1} (0.23% per year or 6.2% per 27-year time span). Over the
412 Sahel, the correlation between W10m and emissions is less strong (R=0.69), but here too,
413 both parameters show a long-term decreasing trend of -0.0052 m s^{-1} (0.13%) per year for
414 W10m and -0.066 g m^{-2} mon^{-1} (0.92%) per year for emission. Accumulated over the 27-
415 year time span, dust emission in Sahel has been reduced significantly by 25%.

NDVI, with a long-term annual mean and standard deviation of 0.18±0.01, is an important dust emission controlling factor over the Sahel. There we see an increasing trend in NDVI until the early 2000s (Figure 8b), after which there appears to vary from year to year but no trend. The trend from 1982 to 2001 is 0.0014 (0.8%) per year, or a change of 13% in NDVI over the two-decade period. This Sahelian NDVI pattern over the 27 years is consistent with previous studies (Tucker et al., 1991; Tucker and Nicholson, 1999; Herrmann et al, 2005; Anyamba et al., 2014). A negative correlation coefficient is found between the changes of emission and NDVI over the Sahel (R=-0.65), but it is negligible over the Sahara (Figure 8b) because the NDVI is almost always below the threshold value of 0.15 there. In both regions, however, the correlation between NDVI and W10m is poor (-0.08 and -0.17 over the Sahara and Sahel, respectively).

The trends of the key parameters are highly dependent on seasons (Figure 9). In the Sahara, the downward trend in W10m and emission, seen in the anomaly of annual mean time series is consistent across three seasons, with only MAM exhibiting no trend. Over the Sahel, the downward trend of W10m and emission is strongest in winter and has no trend in summer. While the correlation coefficient between W10m and emission are high throughout all seasons over the Sahara ($R>0.9$), that over the Sahel is highly variable depending on season ranging from 0.33 in summer to 0.73 in winter (Figure 9a-b). The strong increasing trend of annual NDVI over the Sahel (i.e., Figure 8b) is found in all seasons, but strongest in SON. Similar to the annual analysis (R=-0.17), we find no significant correlation between NDVI and W10m in the seasonal analysis ($-0.37<R<0.24$).

There is little correlation between annual mean NDVI in the Sahara and the Sahel, which is to be expected, given the small and almost invariant NDVI values of the Sahara

(Figure 10a). However, annual mean surface wind in the Sahara and Sahel are connected (R=0.53, Figure 10b) and the emissions and DOD between the Sahara and the Sahel are also positively correlated (R=0.70 for emission and R=0.44 for DOD, Figure 10c and 10d). The long-term average ratio of Sahel DOD to Sahara DOD is 1.3, but this factor has been undergoing a decrease over the period of analysis, so that in recent years DOD over the Sahel and Sahara have been becoming closer in magnitude (Figure 10d). These results suggest that the inter-annual variation of surface wind and thus dust emission are in a coupled system across Northern Africa regardless of NDVI.

4. Discussion

Estimates of dust emission from our area of interest vary widely, depending on the source of information, the specific geographical area, dust particle size range, and time period under investigation. For example, focusing on the Bodélé Depression in northern Chad that falls within the region we define as 'Sahara' a satellite-based estimate gives an emission value of 58 ± 8 Tg $year^{-1}$ (Koren et al., 2006). This represents only 4-5% of the total dust emission that we estimate for the total Sahara from GOCART. Other studies that rely on satellites (Ginoux et al., 2001; Prospero et al., 2002; Ginoux et al., 2012) provide global maps of dust emission, but tabulate the total annual and seasonal estimates from North Africa without distinguishing between the Sahara and Sahel. These estimates of the total North African dust emissions span the range 690-880 Tg $year^{-1}$, about half of our GOCART estimate of 1340-1570 Tg $year^{-1}$. Other techniques to identify dust sources and estimate emissions cause models to vary widely in their estimates. It does not matter whether the comparison is specifically focused on the Bodélé Depression

462 (Todd et al. 2008) or a short observing period (Bou Karam et al., 2009) or covers the
463 entire North Africa region on an annual average (Engelstaederter et al. 2006, see their
464 Table 3.5, Huneeus et al., 2011), or even globally (Textor et al., 2006), the range of
465 estimated dust emissions spans an order of magnitude. Our GOCART values for North
466 Africa fall within but at the upper range of this model diversity.

467 Most dust emission estimates of North Africa do not distinguish between Saharan
468 and Sahelian emission sources, and few attempt to link emissions to environmental
469 factors. An important exception is the previous work targeting dust and dust emission in
470 the Eastern Sahel (10°W-20°E and 10°N-15°N) by Zender and Kwon (2005). They
471 analyzed the annual cycle of dust loading, rainfall, NDVI and surface wind, using the
472 TOMS AOD as a proxy for dust loading, but do not explicitly model the emissions, and
473 they do not explore the long-term variability or trends of these parameters. From their
474 analysis they concluded that precipitation and vegetation together strongly constrain dust
475 and that there is no significant correlation between wind and dust loading over the Sahel.
476 There are two limitations in their analyses. First, given that the Sahel experiences a strong
477 biomass burning season, separating dust from smoke using the AOD involves significant
478 uncertainty. Their attempt to mitigate the contribution from biomass burning aerosol is to
479 limit the analysis to the eastern part of the Sahel during the burning season. This may
480 indeed reduce the uncertainty introduced by the smoke, but it introduces additional
481 uncertainty by excluding a large portion of potential dust sources. Second, dust loading
482 over the Sahel is affected by transport from sources outside of the region, while the
483 emissions that we analyze are not affected by transport. We find that only 40 % of the
484 DOD in winter and 30 % of the DOD in summer over the Sahel originates from dust

485 sources in the Sahel. Thus, using AOD over the Sahel is not the same as focusing on the
486 emissions themselves. In contrast to the Zender and Kwon (2005) conclusion, we find
487 that W10m plays a strong role in dust emission in the Sahel. By examining the full multi-
488 decadal time series, the strong connection between wind and emission, as well as NDVI
489 and emission becomes clear. We note that while both wind and vegetation are correlated
490 to dust emission in the Sahel, wind and vegetation are not correlated with each other
491 (Figure 8). Previous suggestions that vegetation modifies surface wind through roughness
492 considerations are not supported by our results, although our study is done at too coarse a
493 resolution to resolve local scale relationships.

494 Although our study focuses on the relationships between surface wind, NDVI,
495 and dust emission over the Sahara and the Sahel, the importance of the Northern Atlantic
496 sea surface temperature (SST) to the multi-decadal variation of the Sahel rainfall and the
497 wind circulation over the Northern Atlantic-North Africa is well established (Lamb
498 1978a,b, Giannini et al., 2003; Mohino et al., 2011; Martin et al., 2014; Chin et al., 2014).
499 In addition, a previous study has found that the warming trend of North Atlantic SST
500 since the 1980s is strongly tied to a decrease of DOD in the tropical North Atlantic as
501 well as dust concentration at Barbados and Miami (Chin et al., 2014). Although the
502 driving mechanism of the multi-decadal SST variation is still unsettled (Zhang et al.,
503 2013), Atlantic meridional overturning circulation (Delworth and Mann 2000; McCarthy
504 et al., 2015), mid-latitude atmospheric circulation with thermal coupling (Clement et al.,
505 2015), and/or aerosol (Booth et al., 2012) are considered to be associated with the multi-
506 decadal SST variation.

507 There are large differences in dust source locations, strength, and mobilization

schemes (Formenti et al., 2011) as well as wind fields (Menut, 2008) used in different models. In this study, a single NDVI threshold value of 0.15 was chosen across northern Africa to separate the bare desert from the vegetated area in the Sahelian transition zone, following Kim et al. (2013). Kim et al. (2013) pointed out that a ±0.045 change in the current NDVI threshold (i.e., 0.105 or 0.195) will change the bareness area estimate by ±30% and we found a similar sensitivity in the Sahel. Also a relatively coarse resolution (2°×2.5° resolution) for GOCART simulation may cause additional errors in quantitative estimations of dust emissions. The coarse resolution in the global model has difficulties in simulating meso-scale or micro-scale events such as haboobs or dust devils, which are important processes for dust emission (Knippertz and Tood, 2012; Heinold et al., 2013; Marsham et al., 2013; Pantillon et al., 2016). In the present study, the GOCART emission is not sensitive to the change of soil moisture over the Sahara/Sahel region because soil moisture (or surface wetness) enters the emission parameterization as a binary factor. Soil is either dry enough to allow for emission, or it is not. Soil conditions in the MERRA reanalysis over the Sahara/Sahel usually are dry enough to allow continuous dust mobilization. This may contribute additional uncertainties in the model dust emission than when the change of soil moisture is explicitly accounted for in dust emission (e.g., Pierre et al., 2012).

Finally, it should be noted that uncertainties in the MERRA and other reanalysis data sets used for the trend analysis suffer from enhanced uncertainties in this region, due to the lack of surface observations in this area (e.g., Largeron et al., 2015). Largeron et al. (2015) has intensively evaluated surface wind of three global reanalyses (ERA-Interim, NCEP-CFSR and MERRA) using high-frequency observations acquired across the Sahel.

Those reconstructed wind fields are important inputs for many dust emission models. The study found several common challenging issues, but all three reanalyses exhibit insufficient annual cycle, with important seasonally-dependent biases. They all overestimate the surface wind during dry season nights and underestimate it during spring and monsoon season days. The study also found that the reanalyses systematically underestimate the strongest wind speeds, observed in the morning and during deep convective events.

Although previous studies have found that surface observations and various reanalysis data commonly show a decreasing trend of W10m over the Sahel between the 1980s and 2000s, the gradient of the reanalysis data are much weaker than the surface observations (Cowie et al., 2013, Ridley et al., 2014) adding more uncertainties to the reanalysis data.

5. Summary

In this study, we investigated the relationships between surface wind, rainfall, and surface vegetation, all from independent data sets, with global dust model simulations, in a multi-decadal time span from 1982 to 2008. For dust simulations we used the GOCART model with an explicit Sahel area map determined from the AVHRR NDVI.

The magnitude and seasonality of the atmospheric and surface processes vary significantly between the Sahara and the Sahel. The Sahel shows strong rainfall seasonality with the wet season occurring from March to August. NDVI has a peak in September (0.3) and a minimum in June (0.15). The model diagnostics of bareness and source function over the Sahel corresponds with a strong seasonality with a peak in June

554 and minimum in September. A modulating effect of surface vegetation results in a 28 %
555 lower source function in the wet season than the dry season. Monthly mean W10m over
556 the Sahara shows small seasonality, ranging from 4.2 to 4.5 m s^{-1}. Over the Sahel,
557 monthly mean W10m shows much stronger seasonal variation ranging from 3 m s^{-1} in
558 September to 5 m s^{-1} in winter. Unlike the emission, the peak of the Sahel dust loading
559 occurs in April and July, which is similar to the Sahara. The larger loading (i.e., mass per
560 unit area) over the Sahel than the Sahara suggests the dominant source of dust loading
561 over the Sahel is actually transported dust from the North. There are strong regional
562 dependencies in NDVI, bareness, W10m, and emission. Highly positive correlations were
563 found between emission and W10m in both regions, and an anti-correlation between
564 emission and NDVI is found only in the Sahel.
565 The relative contribution of the Sahara and the Sahel to the North Africa and
566 Northern Atlantic dust was estimated from simulations made with the GOCART model
567 and observations. The Sahara is the most dominant dust source emitting 1497 Tg $year^{-1}$,
568 which accounts for 82 % of the North African dust, while the Sahel contributes the
569 remaining 17 %. Unlike the steady wind field throughout the year over the Sahara, over
570 the Sahel more dust is emitted in winter than in summer by a factor of two due to the
571 combined seasonality of wind and vegetation. The GOCART model simulations show
572 that most of the Sahel dust is transported towards the southwest throughout year. This
573 result implies that the Sahel is an important source of dust over the tropical regions
574 during the winter season accounting for 30~40 % of the total in that area. The GOCART
575 model shows a strong latitudinal contrast of the Sahel dust fraction centered at 20°N with

higher values to the south of 20°N, accounting for a quarter of the transatlantic dust reaching South America.

The 27-year time series analysis was conducted for the Sahara and the Sahel from 1982 to 2008. The result showed that i) both W10m and emission exhibit a significant decreasing trend over both regions since the 1980s; ii) NDVI has an increasing trend and is anti-correlated with emission (R=-0.65) over the Sahel, even though NDVI is poorly correlated with W10m (R=-0.05) in that region; iii) emission trends are most clearly dependent on W10m in both the Sahara (R=0.92) and the Sahel (R=0.69); and iv) W10m trends in the two regions are linked with a positive correlation (R=0.53). Although vegetation plays a modulating role to the long-term trends and seasonal cycle of dust emission over the Sahel, our results suggest that North African dust loading and its inter-annual variation is governed by the coupled North African circulation system that produces the surface wind.

The take home message from our analysis is that dust emission in the Sahara is controlled completely by the wind, while dust emission in the Sahel is controlled by the wind but modified by the vegetation coverage. Both regions have been declining in dust emission over the past three decades, mostly due to the decrease in near surface wind speed during this time period. The Sahel is an important dust source to the dust loading over the tropical Atlantic and the shores of South America, but ironically most of the dust loading directly above the Sahel is not of local origin but transported from the Sahara and other locations.

The multi-decadal model simulations combined with reanalysis data and satellite NDVI observations allows new insight into the long-term correlated trends of the wind,

surface vegetation, and dust emission over the Sahara and Sahel. Previous studies have noted a decrease in dust loading across the northern Atlantic, including a decrease in surface dust concentration at Barbados. Analysis of the parameters affecting dust loading shows widespread changes in surface wind speed, vegetation, and subsequent emission at the sources. This decrease originates over North Africa, affecting emission sources in both the Sahara and Sahel, and is not a simple shifting of wind patterns or deposition process over the ocean. Identifying the cause of these widespread changes lies beyond the scope of the present study, but are key to understanding regional scale climate variability.

Acknowledgements

This work is supported by NASA Modeling, Analysis and Prediction (MAP) and EOS Programs. We would like to thank the MISR, MODIS, and AERONET team for the data used in this study. William Stockwell thanks the National Aeronautics and Space Administration for the grant "Howard University Beltsville Center for Climate System Observation" and a grant from the National Oceanic and Atmospheric Administration to Howard University's NOAA Center for Atmospheric Sciences for supporting his participation in this work.

References

Anyamba, A., Small, J. L., Tucker, C. J., Pak, E. W., 2014. Thirty-two Years of Sahelian Zone Growing Season Non-Stationary NDVI3g Patterns and Trends. Remote Sens. 6, 3101-3122.

Beck, C., Grieser, J., Rudolf, B., 2005. A New Monthly Precipitation Climatology for the Global Land Areas for the Period 1951 to 2000; Klimastatusbericht KSB 2004; DWD: Offenbach, Germany. Available online: ftp://ftp-anon.dwd.de/pub/data/gpcc/PDF/pdf_28_precipitation.pdf (accessed on 18 November 2015).

Bichet, A., Wild, M., Folini, D., Schär, C., 2012. Causes for decadal variations of wind speed over land: Sensitivity studies with a global climate model. Geophys. Res. Lett. 39, L11701. doi:10.1029/2012GL051685.

Booth, B. B. B., Dunstone, N. J., Halloran, P. R., Andrews, T., Bellouin, N., 2012. Aerosols implicated as a prime driver of twentieth-century North Atlantic climate variability. Nature 484, 228–232.

Bou Karam, D., Flamant, C., Tulet, P., Chaboureau, J.-P., Dabas, A., and Todd, M. C., 2009. Estimate of Sahelian dust emissions in the intertropical discontinuity region of the West African Monsoon. J. Geophys. Res. 114, D13106. doi:10.1029/2008JD011444.

Brown, M. E., Pinzon, J. E., Didan, K., Morisette, J. T., Tucker, C. J., 2006. Evaluation of the consistency of long-term NDVI time series derived from AVHRR, SPOT-Vegetation, SeaWIFS, MODIS and LandSAT ETM+. IEEE Transactions Geoscience and Remote Sensing 44, 1787-1793.

Carlson, T. N., and Prospero, J. M., 1972. The Large-scale movement of Saharan air outbreaks of the Northern Equatorial Atlantic. J. Appl. Meteorol. 11, 283-297.

Charney, J. G., 1975. Dynamics of deserts and drought in Sahel. Quart. J. Roy. Meteor. Soc. 101, 193–202.

Chin, M., Ginoux, P., Kinne, S., Torres, O., Holben, B. N., Duncan, B. N., Martin, R. V., Logan, J. A., Higurashi, A., Nakajima, T., 2002. Tropospheric aerosol optical thickness from the GOCART model and comparisons with satellite and Sun photometer measurements. J. Atmos. Sci. 59(3), 461–483.

Chin, M., Diehl, T., Ginoux, P., Malm, W., 2007. Intercontinental transport of pollution and dust aerosols: Implications for regional air quality. Atmos. Chem. Phys. 7, 5501–5517.

Chin, M., Diehl, T., Dubovik, O., Eck, T. F., Holben, B. N., Sinyuk, A., Streets, D. G., 2009. Light absorption by pollution, dust and biomass burning aerosols: A global model study and evaluation with AERONET data. Ann. Geophys. 27, 3439-3464.

Chin, M. Diehl, T., Tan, Q., Prospero, J. M., Kahn, R. A., Remer, L. A., Yu, H., Sayer, A. M., Bian, H., Geogdzhayev, I. V., Holben, B. N., Howell, S. G., Huebert, B. J., Hsu, N. C., Kim, D., Kucsera, T. L., Levy, R. C., Mishchenko, M. I., Pan, X., Quinn, P. K., Schuster, G. L., Streets, D. G., Strode, S. A., Torres, O., and Zhao, X.-P., 2014. Multi-

decadal aerosol variations from 1980 to 2009: a perspective from observations and a global model. Atmos. Chem. Phys. 14, 3657-3690. doi:10.5194/acp-14-3657-2014.

Clement, A., Bellomo, K., Murphy, L. N., Cane, M. A., Mauritsen, T., Radel, G., Stevens, B., 2015. The Atlantic Multidecadal Oscillation without a role for ocean circulation. Science 350, 320-324. doi:10.1126/science.aab3980.

Cowie, S. M., Knippertz, P., Marsham, J. H., 2013. Are vegetation related roughness changes the cause of the recent decrease in dust emission from the Sahel?. Geophys. Res. Lett. 40, 1868–1872. doi:10.1002/grl.50273.

Delworth, T. L., Mann, M. E., 2000. Observed and simulated multidecadal variability in the Northern Hemisphere. Climate Dyn. 16, 661–676.

Dubovik, O., Smirnov, A., Holben, B. N., King, M. D., Kaufman, Y. J., Eck, T. F., Slutsker, I., 2000. Accuracy assessments of aerosol optical properties retrieved from Aerosol Robotic Network (AERONET) Sun and sky radiance measurements. J. Geophys. Res. 105, 9791–9806.

Dubovik, O., Holben, B. N., Eck, T. F., Smirnov, A., Kaufman, Y. J., King, M. D., Tanré, D., Slutsker, I., 2002. Variability of absorption and optical properties of key aerosol types observed in worldwide locations. J. Atmos. Sci. 59, 590–608.

Dubovik, O., Sinyuk, A., Lapyonok, T., Holben, B. N., Mishchenko, M., Yang, P., Eck, T. F., Volten, H., Munoz, O., Veihelmann, B., van der Zande, W. J., Leon, J.-F., Sorokin, M., and Slutsker, I., 2006. Application of spheroid models to account for aerosol particle nonsphericity in remote sensing of desert dust. J. Geophys. Res. 111, D11208. doi:10.1029/2005JD006619.

Eck, T. F., Holben, B. N., Sinyuk, A., Pinker, R. T., Goloub, P., Chen, H., Chatenet, B., Li, Z., Singh, R. P., Tripathi, S. N., Reid, J. S., Giles, D. M., Dubovik, O., O'Neill, N. T., Smirnov, A., Wang, P., Xia, X., 2010. Climatological aspects of the optical properties of fine/coarse mode aerosol mixtures. J. Geophys. Res. 115, D19205. doi:10.1029/2010JD014002.

Engelstaedter, S., Tegen, I., Washington, R., 2006. North African dust emissions and transport. Earth-Sci. Rev. 79 (1), 73–100.

Evan, A. T., Heidinger, A. K., Bennartz, R., Bennington, V., Mahowald, N. M., Corrada-Bravo, H., Velden, C. S., Myhre, G., Kossin, J. P., 2008. Ocean temperature forcing by aerosols across the Atlantic tropical cyclone development region. Geochem. Geophy. Geosy. 9, Q05V04. doi:10.1029/2007GC001774.

Foltz, G. R., McPhaden, M. J., 2008. Trends in Sahara dust and tropical Atlantic climate during 1980-2006. Geophys. Res. Lett. 35, L20706. DOI: 10.1029/2008GL035042.

Formenti, P., Schütz, L., Balkanski, Y., Desboeufs, K., Ebert, M., Kandler, K., Petzold, A., Scheuvens, D., Weinbruch, S., Zhang, D., 2011. Recent progress in understanding physical and chemical properties of African and Asian mineral dust. Atmos. Chem. Phys. 11, 8231-8256. doi:10.5194/acp-11-8231-2011.

Forster, P., Ramaswamy, V., Artaxo, P., Berntsen, T., Betts, R., Fahey, D. W., Haywood, J., Lean, J., Lowe, D. C., Myhre, G., Nganga, J., Prinn, R., Raga, G., Schulz, M., and Van

700 Dorland, R., 2007. Changes in Atmospheric Constituents and in Radiative Forcing, in:
701 Climate Change 2007: *The Physical Science Basis, contribution of Working Group I to*
702 *the Fourth Assessment Report of the Intergovernmental Panel on Climate Change*, edited
703 by: Solomon, S. D., Qin, M., Manning, Z., Chen, M., Marquis, K. B., Averyt, M. T., and
704 Miller, H. L., Cambridge University Press, Cambridge, United Kingdom and New York,
705 NY, USA, 129–234.

706 Giannadaki, D., Pozzer, A., Lelieveld, J., 2014. Modeled global effects of airborne desert
707 dust on air quality and premature mortality. Atmos. Chem. Phys. 14, 957-968.
708 doi:10.5194/acp-14-957-2014.

709 Giannini, A., Saravanan, R., Chang, P., 2003. Oceanic forcing of Sahel rainfall on
710 interannual to interdecadal time scales. Science 302, 1027–1030.

711 Ginoux, P., Chin, M., Tegen, I., Prospero, J. M., Holben, B., Dubovik, O., Lin, S. J., 2001.
712 Sources and distributions of dust aerosols simulated with the GOCART model. J.
713 Geophys. Res. 106(D17), 20255–20273.

714 Ginoux, P., Prospero, J. M., Torres, O., and Chin, M., 2004. Long-term simulation of
715 global dust distribution with the GOCART model: Correlation with the North Atlantic
716 Oscillation. Environ. Model. Software 19, 113-128. doi:10.1016/S1364-8152(03)00114-2.

717 Ginoux, P., Prospero, J. M., Gill, T. E., Hsu, N. C., and Zhao, M., 2012. Global-scale
718 attribution of anthropogenic and natural dust sources and their emission rates based on
719 MODIS Deep Blue aerosol products. Rev. Geophys. 50, RG3005.
720 doi:10.1029/2012RG000388.

721 Guo, Y., Tian, B., Kahn, R. A., Kalashnikova, O., Wong, S., Waliser, D. E., 2013.
722 Tropical Atlantic dust and smoke aerosol variations related to the Madden-Julian
723 Oscillation in MODIS and MISR observations. J. Geophys. Res. 118, 4947–4963.
724 doi:10.1002/jgrd.50409.

725 Haywood, J. M., Francis, P., Osborne, S., Glew, M., Loeb, N., Highwood, E., Tanre, D.,
726 Myhre, G., Formenti, P., and Hirst, E., 2003. Radiative properties and direct radiative
727 effect of Saharan dust measured by the C-130 aircraft during SHADE: 1. Solar spectrum.
728 J. Geophys. Res. 108(D18), 8577. doi:10.1029/2002JD002687.

729 Heinold, B., Knippertz, P., Marsham, J., Fiedler, S., Dixon, N., Schepanski, K., Laurent,
730 B., Tegen, I., 2013. The role of deep convection and nocturnal low-level jets for dust
731 emission in summertime West Africa: Estimates from convection-permitting simulations.
732 J. Geophys. Res. 118, 4385–4400. doi:10.1002/jgrd.50402.

733 Herrmann, S. M., Anyamba, A., Tucker, C. J., 2005. Recent trends in vegetation
734 dynamics in the African Sahel and their relationship to climate. Global Environ. Change
735 15, 394–404.

736 Holben, B. N., Eck, T. F., Slutsker, I., Tanre, D., Buis, J. P., Setzer, A., Vermote, E.,
737 Reagan, J. A., Kaufman, Y. J., Nakajima, T., Lavenu, F., Jankowiak, F., Smirnov, A.,
738 1998. AERONET - A federated instrument network and data archive for aerosol
739 characterization. Rem. Sens. Environ. 66, 1-16.

740 Huneeus, N., Schulz, M., Balkanski, Y., Griesfeller, J., Prospero, J., Kinne, S., Bauer, S.,
741 Boucher, O., Chin, M., Dentener, F., Diehl, T., Easter, R., Fillmore, D., Ghan, S., Ginoux,
742 P., Grini, A., Horowitz, L., Koch, D., Krol, M. C., Landing, W., Liu, X., Mahowald, N.,
743 Miller, R., Morcrette, J.-J., Myhre, G., Penner, J., Perlwitz, J., Stier, P., Takemura, T.,
744 and Zender, C. S., 2011. Global dust model intercomparison in AeroCom phase I. Atmos.
745 Chem. Phys. 11, 7781–7816. doi:10.5194/acp-11-7781-2011.

746 Jickells, T. D., An, Z. S., Andersen, K. K., Baker, A. R., Berga- metti, G., Brooks, N.,
747 Cao, J. J., Boyd, P. W., Duce, R. A., Hunter, K. A., Kawahata, H., Kubilay, N., laRoche,
748 J., Liss, P. S., Mahowald, N., Prospero, J. M., Ridgwell, A. J., Tegen, I., and Torres, R.,
749 2005. Global iron connections between desert dust, ocean biogeochemistry, and climate.
750 Science 308(5718), 67–71.

751 Kahn, R. A., Gaitley, B., Martonchik, J., Diner, D., Crean, K., Holben, B., 2005. MISR
752 global aerosol optical depth validation based on two years of coincident AERONET
753 observations. J. Geophys. Res. 110, D10S04. doi:10.1029/2004JD004706.

754 Kaufman, Y. J., Koren, I., Remer, L. A., Tanré, D., Ginoux, P., Fan, S., 2005. Dust
755 transport and deposition observed from the Terra-Moderate Resolution Imaging
756 Spectroradiometer (MODIS) spacecraft over the Atlantic Ocean. J. Geophys. Res. 110,
757 D10S12. doi:10.1029/2003JD004436.

758 Kim, K.-M, Lau, W.-K., Sud, Y. C., and Walker, G. K., 2010. Influence of aerosol-
759 radiative forcings on the diurnal and seasonal cycles of rainfall over West Africa and
760 Eastern Atlantic Ocean using GCM simulations. Climate Dynamics 11, 115-126.
761 doi:10.1007/s00382-010- 0750-1.

762 Kim, D., Chin, M., Bian, H., Tan, Q., Brown, M., Zheng, T., You, R., Diehl, T., Ginoux,
763 P., Kucsera T., 2013. The Effect of the Dynamic Surface Bareness on Dust Source
764 Function, Emission, and Distribution. J. Geophy. Res. 118, 871-886.
765 doi:10.1029/2012JD017907.

766 Kim, D., Chin, M., Yu, H. , Diehl, T., Tan, Q., Tsigaridis, K., Bauer, S. E., Takemura, T.,
767 Pozzoli, L., Bellouin, N., Schulz, M., Peyridieu, S., Chédin, A., 2014. Source, sinks, and
768 transatlantic transport of North African dust aerosol: A multi-model analysis and
769 comparison with remote-sensing data. J. Geophy. Res. 119, 6259–6277. doi:10.1002/
770 2013JD021099.

771 Kinne, S., Schulz, M., Textor, C., Guibert, S., Balkanski, Y., Bauer, S. E., Berntsen, T.,
772 Berglen, T. F., Boucher, O., Chin, M., Collins, W., Dentener, F., Diehl, T., Easter, R.,
773 Feichter, J., Fillmore, D., Ghan, S., Ginoux, P., Gong, S., Grini, A., Hendricks, J., Herzog,
774 M., Horowitz, L., Kottek, I., Grieser, M., J., Beck, C., Rudolf, B., Rubel, F., 2006. World
775 map of the Köppen-Geiger climate classification updated. Meteorol. Z. 15, 259–263.

776 Klose, M., Shao, Y., Karremann, M. K., Fink, A. H., 2010. Sahel dust zone and synoptic
777 background. Geophys. Res. Lett. 37, L09802. doi:10.1029/2010GL042816.

778 Knippertz, P., Todd, M. C., 2012. Mineral dust aerosols over the Sahara: Meteorological
779 controls on emission and transport and implications for modeling. Rev. Geophys. 50,
780 RG1007. doi:10.1029/2011RG000362.

781 Koren, I., Kaufman, Y. J., Washington, R., Todd, M. C., Rudich, Y., Vanderlei Martins,
782 J., and Rosenfeld, D., 2006. The Bodélé depression: a single spot in the Sahara that

783 provides most of the mineral dust to the Amazon forest. Environ. Res. Lett. 1, 014005.
784 doi:10.1088/1748-9326/1/1/014005.

785 Kottek, M., Grieser, J., Beck, C., Rudolf, B., Rubel, and F., 2006. World map of the
786 Köppen–Geiger climate classification updated. Meteorologische Zeitschrift 15, 259–263.

787 Lamb, P. J. 1978a. Case studies of tropical Atlantic surface circulation patterns during
788 recent sub-Saharan weather anomalies: 1967 and 1968. Mon. Wea. Rev. 106, 482–491.

789 Lamb, P. J. 1978b. Large-scale tropical Atlantic surface circulation patterns associated
790 with subsaharan weather anomalies. Tellus 30, 240–251.

791 Largeron, Y., Guichard, F., Bouniol, D., Couvreux, F., Kergoat, L., Marticorena B., 2015.
792 Can we use surface wind fields from meteorological reanalyses for Sahelian dust
793 emission simulations?. Geophys. Res. Lett. 42, 2490-2499. doi: 10.1002/2014GL062938.

794 Levy, R. C., Remer, L. A., Kleidman, R. G., Mattoo, S., Ichoku, C., Kahn, R., Eck, T. F.,
795 2010. Global evaluation of the Collection 5 MODIS dark-target aerosol products over
796 land. Atm. Chem. Phys. 10, 10399–10420.

797 Maher, B. A., Prospero, J. M., Mackie, D., Gaiero, D., Hesse, P., Balkanski, Y., 2010.
798 Global connections between aeolian dust, climate and ocean biogeochemistry at the
799 present day and at the last glacial maximum. Earth-Science Reviews 99, 61–97.
800 doi:10.1016/j.earscirev.2009.12.001.

801 Mahowald, N. M., Kloster, S., Engelstaedter, S., Moore, J. K., Mukhopadhyay, S.,
802 McConnell, J. R., Albani, S., Doney, S. C., Bhattacharya, A., Curran, M. A. J., Flanner,
803 M. G., Hoffman, F. M., Lawrence, D. M., Lindsay, K., Mayewski, P. A., Neff, J.,
804 Rothenberg, D., Thomas, E., Thornton, P. E. and Zender, C. S., 2010. Observed 20th
805 century desert dust variability: Impact on climate and biogeochemistry. Atmos. Chem.
806 Phys. 10, 10875-10893. doi:10.5194/acp-10-10875-2010.

807 Marsham, J. H., Dixon, N. S., Garcia-Carreras, L., Lister, G., Parker, D. J., Knippertz, P.,
808 Birch, C. E., 2013. The role of moist convection in the West African monsoon system:
809 Insights from continental-scale convection-permitting simulations. Geophys. Res. Lett.
810 40, 1843–1849. doi:10.1002/grl.50347.

811 Martin, E. R., Thorncroft, C., Booth, B. B. B., 2014. The Multidecadal Atlantic SST—
812 Sahel Rainfall Teleconnection in CMIP5 Simulations. J. Climate 27, 784–806.

813 McCarthy, G. D., Haigh, I. D., Hirschi, J. J.-M., Grist, J. P., Smeed, D. A., 2015. Ocean
814 impact on decadal climate revealed by sea level. Nature 521, 508–510.

815 Menut, L. 2008. Sensitivity of hourly Saharan dust emissions to NCEP and ECMWF
816 modeled wind speed. J. Geophys. Res. 113, D16201. doi:10.1029/2007JD009522.

817 Mohino, E., Janicot, S., Bader, J., 2011. Sahel rainfall and decadal to multidecadal sea
818 surface temperature variability. Clim. Dyn. 37, 419-440.

819 Pantillon, F., Knippertz, P., Marsham, J. H., Panitz, H.-J., Bischoff-Gauss, I., 2016.
820 Modeling haboob dust storms in large-scale weather and climate models. J. Geophys. Res.
821 121, 2090-2109. doi:10.1002/2015JD024349.

Pierre, C., Bergametti, G., Marticorena, B., Mougin, E., Bouet, C., Schmechtig, C., 2012. Impact of vegetation and soil moisture seasonal dynamics on dust emissions over the Sahel. J. Geophys. Res. 117, D06114. doi:10.1029/2011JD016950.

Pinzon, J. E., Tucker, C. J , 2014. A non-stationary 1981–2012 AVHRR NDVI3g time series. Remote Sens. 6, 6929–6960.

Prospero, J. M., Ginoux, P., Torres, O., Nicholson, S. E., and Gill, T. E., 2002. Environmental characterization of global sources of atmospheric soil dust identified with the Nimbus 7 Total Ozone Mapping Spectrometer (TOMS) absorbing aerosol product. Rev. Geophys. 40, 1002. doi:10.1029/2000RG000095.

Prospero, J. M., Lamb, P. J., 2003. African droughts and dust transport to the Caribbean: Climate change implications. Science 302(5647), 1024–1027.

Prospero, J. M., Collard, F.-X., Molinié, J., Jeannot, A., 2014. Characterizing the annual cycle of African dust transport to the Caribbean Basin and South America and its impact on the environment and air quality. Global Biogeochem. Cycles 29, 757–773. doi:10.1002/2013GB004802.

Reichle, R. H., Koster, R. D., De Lannoy, G. J. M., Forman, B. A., Liu, Q., Mahanama, S. P. P., and Toure, A., 2011. Assessment and enhancement of MERRA land surface hydrology estimates. J. Clim. 24, 6322-6338. doi:10.1175/JCLI-D-10-05033.1.

Remer, L. A., Kaufman, Y. J., Tanré, D., Mattoo, S., Chu, D. A., Martins, J. V., Li, R.-R., Ichoku, C., Levy, R. C., Kleidman, R. G., Eck, T. F., Vermote, E. and Holben, B. N., 2005. The MODIS aerosol algorithm, products, and validation. J. Atmos. Sci. 62, 947-973. doi:10.1175/JAS3385.1.

Ridley, D. A., Heald, C. L., Prospero, J. M., 2014. What controls the recent changes in African mineral dust aerosol across the Atlantic?. Atmos. Chem. Phys. 14, 5735-5747. doi:10.5194/acp-14-5735-2014.

Rienecker, M. M., Suarez, M. J., Gelaro, R., Todling, R., Bacmeister, J., Liu, E., Bosilovich, M. G., Schubert, S. D., Takacs, L., Kim, G.-K., Bloom, S., Chen, J., Collins, D., Conaty, A., da Silva, A., Gu, W., Joiner, J., Koster, R. D., Lucchesi, R., Molod, A., Owens, T., Pawson, S., Pegion, P., Redder, C. R., Reichle, R., Robertson, F. R., Ruddick, A. G., Sienkiewicz, M. and Woollen, J., 2011. MERRA: NASA's Modern-Era Retrospective Analysis for Research and Applications. J. Climate 24, 3624–3648. doi:10.1175/JCLI-D-11-00015.1.

Shao, Y., Fink, A. H., and Klose, M., 2010. Numerical simulation of a continental-scale Saharan dust event. J. Geophys. Res. 115, D13205. doi:10.1029/2009JD012678.

Tegen, I., Fung, I., 1994, Modeling of mineral dust in the atmosphere: Sources, transport, and optical thickness. J. Geophys. Res. 99, 22897-22914.

Tegen, I., Werner, M., Harrison, S. P., Kohfeld, K. E., 2004. Relative importance of climate and land use in determining present and future global soil dust emission. Geophys. Res. Lett. 31, L05105. doi:05110.01029/02003GL019216.

Textor, C., Schulz, M., Guibert, S., Kinne, S., Balkanski, Y., Bauer, S., Berntsen, T., Berglen, T., Boucher, O., Chin, M., Dentener, F., Diehl, T., Easter, R., Feichter, H.,

Fillmore, D., Ghan, S., Ginoux, P., Gong, S., Grini, A., Hendricks, J., Horowitz, L., Huang, P., Isaksen, I., Iversen, I., Kloster, S., Koch, D., Kirkev°ag, A., Kristjansson, J. E., Krol, M., Lauer, A., Lamarque, J. F., Liu, X., Montanaro, V., Myhre, G., Penner, J., Pitari, G., Reddy, S., Seland, Ø., Stier, P., Takemura, T., and Tie, X., 2006. Analysis and quantification of the diversities of aerosol life cycles within AeroCom. Atmos. Chem. Phys. 6, 1777–1813. doi:10.5194/acp-6-1777-2006.

Todd, M. C., Bou Karam, D., Cavazos, C., Bouet, C., Heinold, B., Baldasano, J. M., Cautenet, G., Koren, I., Perez, C., Solmon, F., Tegen, I., Tulet, P., Washington, R., and Zakey, A., 2008. Quantifying uncertainty in estimates of mineral dust flux: An intercomparison of model performance over the *Bodélé* Depression, northern Chad. J. Geophys. Res. 113, D24107. doi:10.1029/2008JD010476.

Tucker, C. J., Dregne, H. E., Newcomb, W. W., 1991. Expansion and Contraction of the Sahara Desert from 1980 to 1990. Science 253, 299-301.

Tucker, C. J., Nicholson, S. E., 1999. Variations in the size of the Sahara desert from 1980 to 1997. Ambio 28(7), 587-591.

Tucker, C. J., Pinzon, J. E., Brown, M. E., Slayback, D., Pak, E. W., Mahoney, R., Vermote, E., El Saleous, N., 2005. An extended AVHRR 8-km NDVI data set compatible with MODIS and SPOT vegetation NDVI data. Int. J. Remote Sens. 26, 4485–4498.

Vautard, R., Cattiaux, J., Yiou, P., Thépaut, J.-N., Ciais, P., 2010. Northern Hemisphere atmospheric stilling partly attributed to an increase in surface roughness. Nature Geoscience 3, 756–761. doi:10.1038/ngeo979.

Wang, C., Dong, S., Evan, A. T., Foltz, G. R., Lee S.-K., 2012. Multidecadal covariability of North Atlantic sea surface temperature, African dust, Sahel rainfall, and Atlantic hurricanes. J. Climate 25, 5404–5415.

Yoshioka, M., Mahowald, N., Conley, A., Collins, W., Fillmore, D., and Coleman, D., 2007. Impact of desert dust radiative forcing on Sahel precipitation: relative importance of dust compared to sea surface temperature variations, vegetation changes and greenhouse gas warming. J. Climate 20, 1445–1467.

Yu, H., Chin, M., Remer, L. A., Kleidman, R. G., Bellouin, N., Bian, H., and Diehl, T., 2009. Variability of marine aerosol fine-mode fraction and estimates of anthropogenic aerosol component over cloud-free oceans from the Moderate Resolution Imaging Spectroradiometer (MODIS). J. Geophys. Res. 114, D10206. doi:10.1029/2008JD010648.

Yu, H., Chin, M., Yuan, T., Bian, H., Remer, L. A., Prospero, J. M., Omar, A., Winker, D., Yang, Y., Zhang, Y., Zhang, Z., Zhao, C., 2015a. The fertilizing role of African dust in the Amazon rainforest: A first multiyear assessment based on data from Cloud-Aerosol Lidar and Infrared Pathfinder Satellite Observations. Geophys. Res. Lett. 42, 1984-1991. doi:10.1002/2015GL063040.

Yu, H., Chin, M., Bian, H., Yuan, T., Prospero, J. M., Omar, A. H., Remer, L. A., Winker, D. M., Yang, Y., Zhang, Y., Zhang, Z., 2015b. Quantification of trans-Atlantic dust transport from seven-year (2007-2013) record of CALIPSO lidar measurements. Remote Sen. Environ. 159, 232-249. doi:10.1016/j.rse.2014.12.010.

Zender, C. S., Kwon, E. Y., 2005. Regional contrasts in dust emission responses to

905 climate. J. Geophys. Res. *110*, D13201. doi:10.1029/2004JD005501.

906 Zhang, R., Delworth, T. L., Sutton, R., Hodson, D. L. R., Dixon, K. W., Held, I. M.,
907 Kushnir, Y., Marshall, J., Ming, Y., Msadek, R., Robson, J., Rosati, A. J., Ting, M.,
908 Vecchi, G. A., 2013. Have Aerosols Caused the Observed Atlantic Multidecadal
909 Variability?. J. Atmos. Sci. 70, 1135–1144.

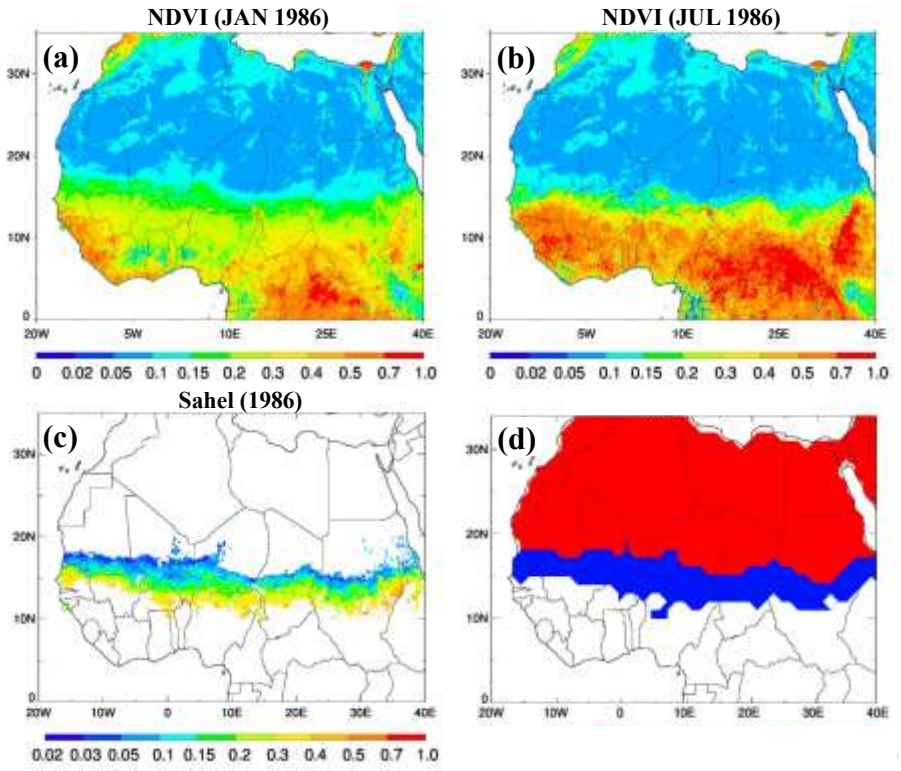

Figure 1. Distribution of (a) January and (b) July NDVI in 1986. The Bodélé depression is located at 17°N,18E°. (c) Distribution of the area where $NDVI_{min}$ <0.15 and $NDVI_{max}$>0.2 between 10°N-20°N. (d) Climatological map of Sahel in blue and Sahara in red determined from 1982-2008 NDVI data.

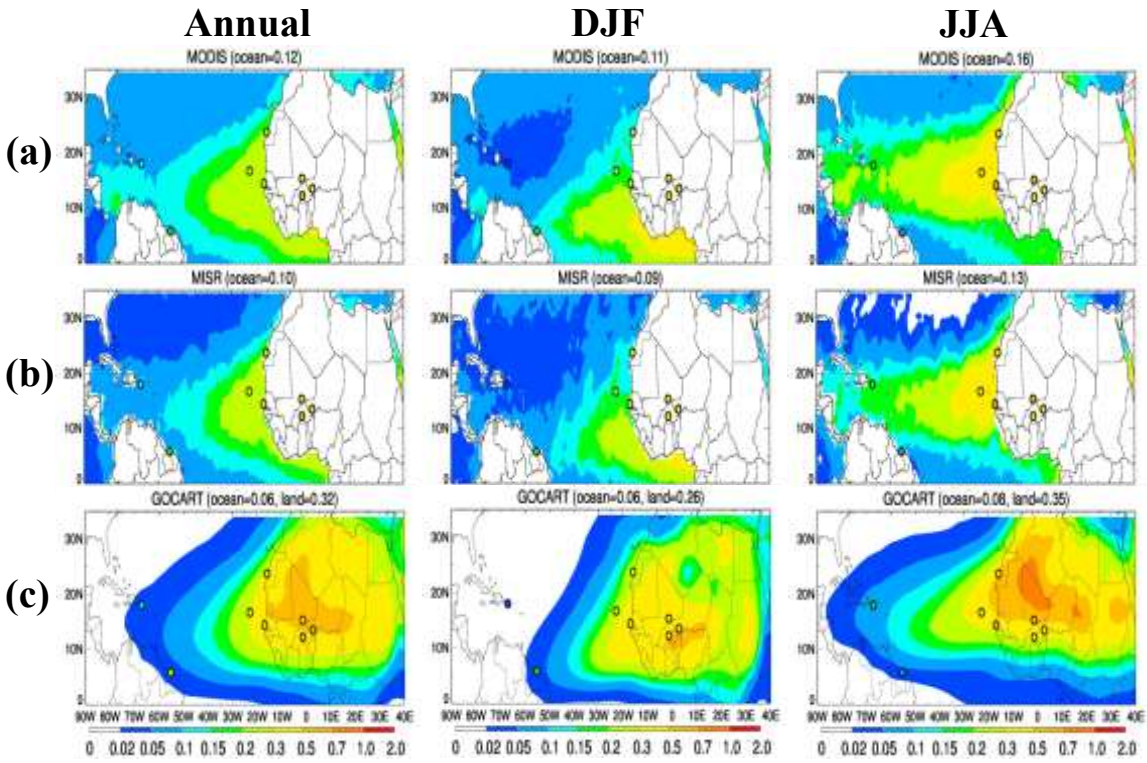

Figure 2. DOD from (a) MODIS and (b) MISR over ocean and (c) GOCART-base simulation over both land and ocean averaged for 2001-2007. DODs from 8 AERONET stations for 2001-2007 are shown in colored circles. Mean DOD values are indicated in the parenthesis.

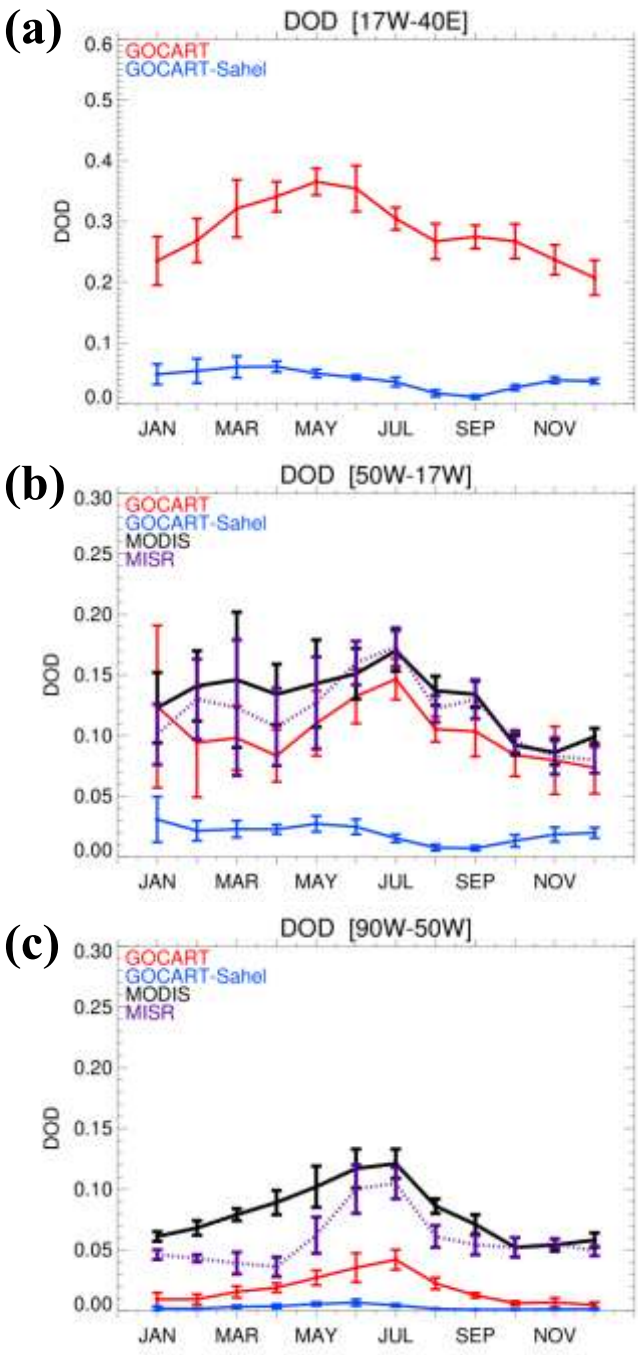

Figure 3. (a) Dust optical depth (DOD) from GOCART, averaged for 2001-2007 over the land portion of the entire domain (0°-35°N, 17°W-40°E). GOCART-Sahel is DOD emitted only from the Sahel with all other dust source locations turned off. (b, c) Same as (a), except for ocean only and divided into Eastern and Western sections of (50°W-17°W) and (90°W-50°W), respectively. Dust optical depth from MODIS and MISR averaged for 2001-2007 are also plotted over oceanic domains in (b, c). Error bars represent standard deviations of monthly DOD in 2001-2007.

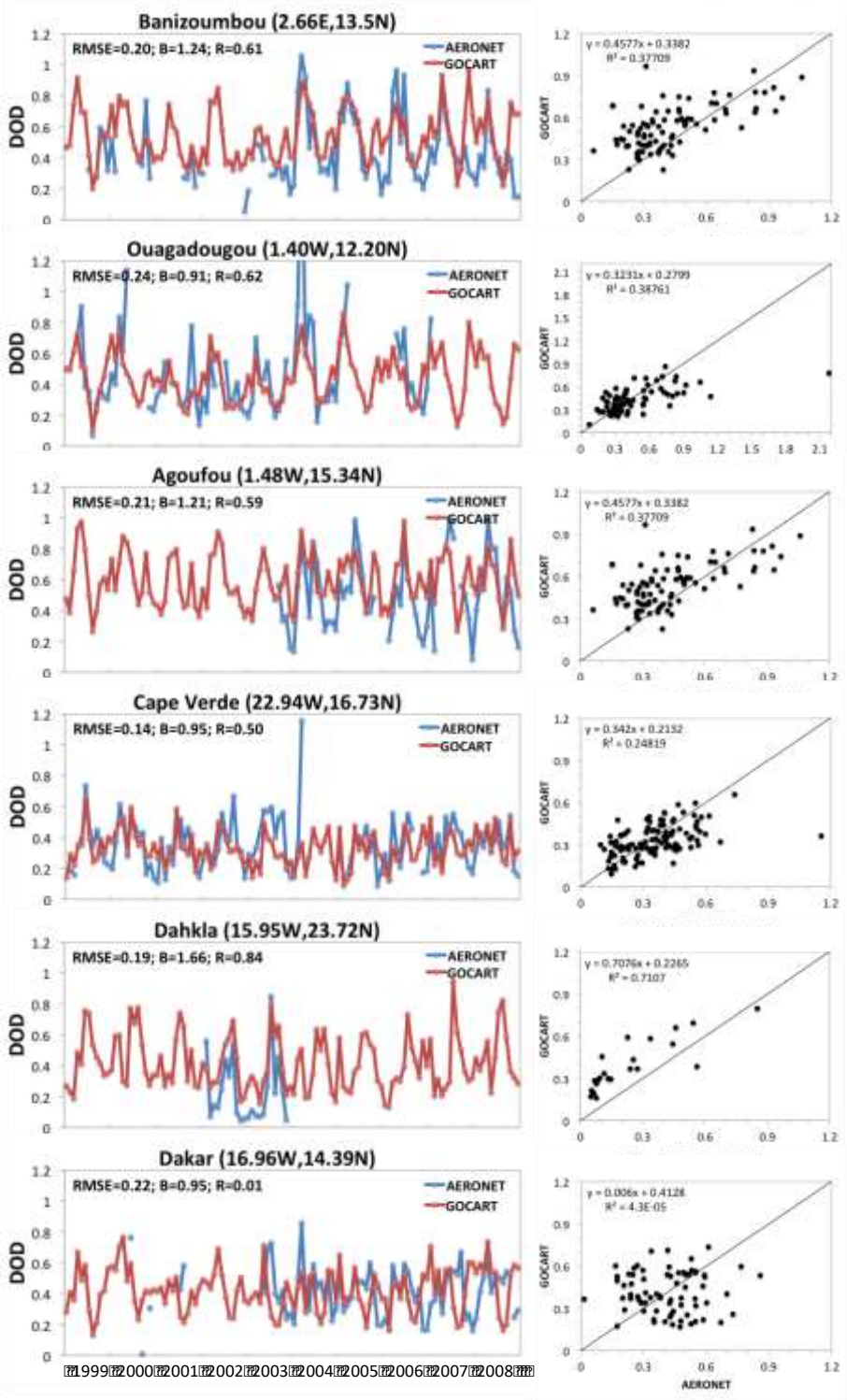

Figure 4. (left column) Monthly-mean time series of dust optical depth at the six stations over the Sahel for 1999-2008 and (right column) its scatter plot. The coarse-mode aerosol optical depth is used as a proxy of DOD for AERONET observation. Numbers in the figure include root mean square error (RMSE), mean bias (B), and correlation coefficient (R) between model and observations.

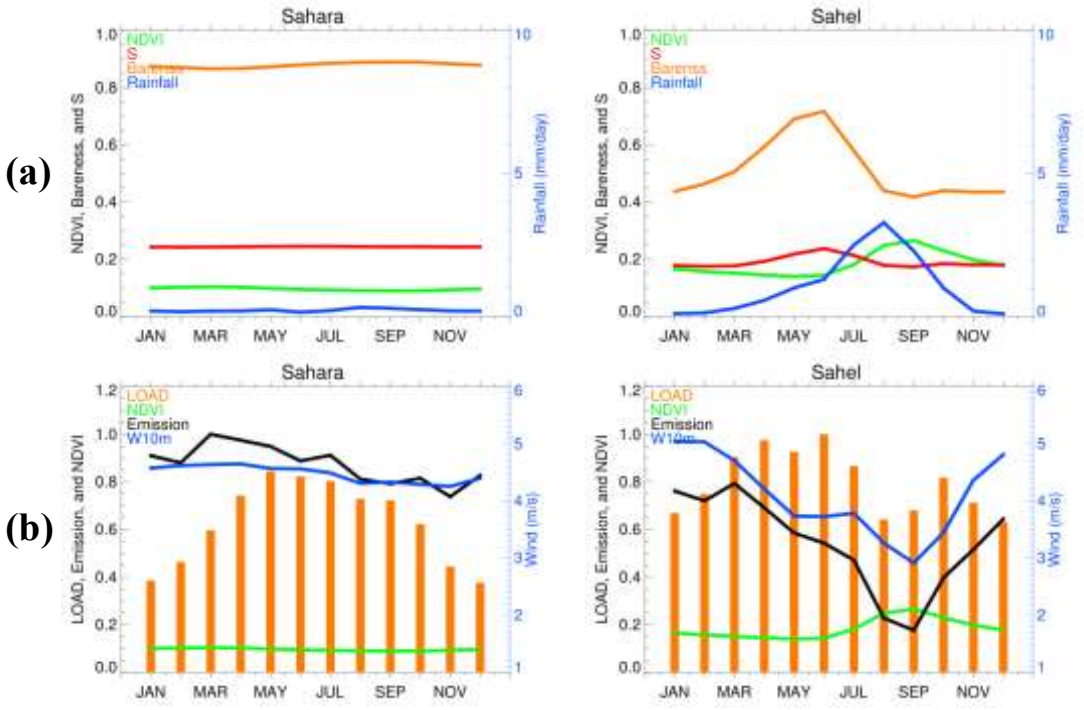

Figure 5. (a) Monthly values of rainfall, NDVI, bareness, and source function and (b) W10m, S, dust emission, and dust loading over the Sahara (left) and Sahel (right) averaged from 1982-2008. Emission and loading are normalized to their maximum values in North Africa of 1.22×10^{7} g km^{-2} mon^{-1} and 10.1 g km^{-2}, respectively.

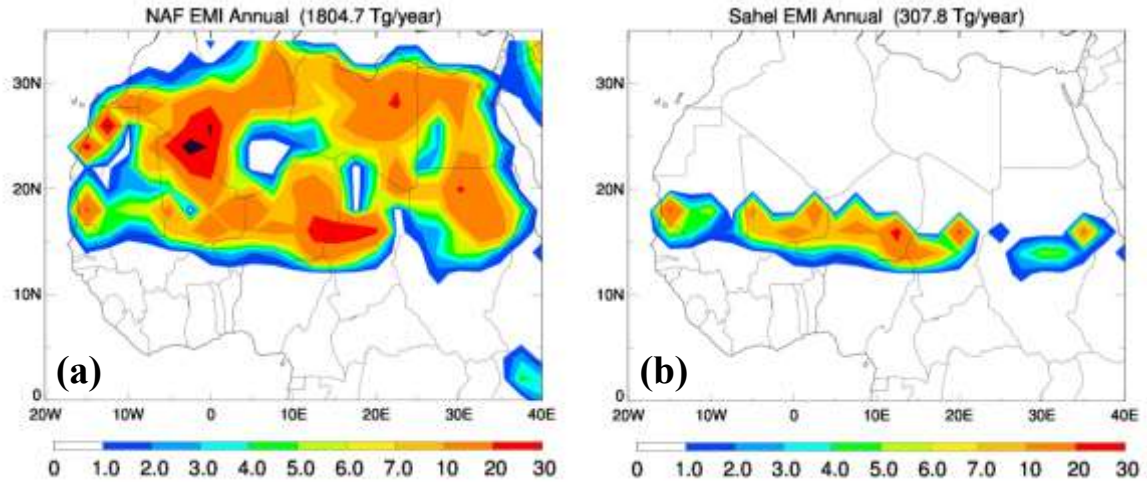

Figure 6. Distribution of modeled dust emission from (a) North Africa and (b) Sahel, averaged for 1982-2008. NAF refers to all of North Africa.

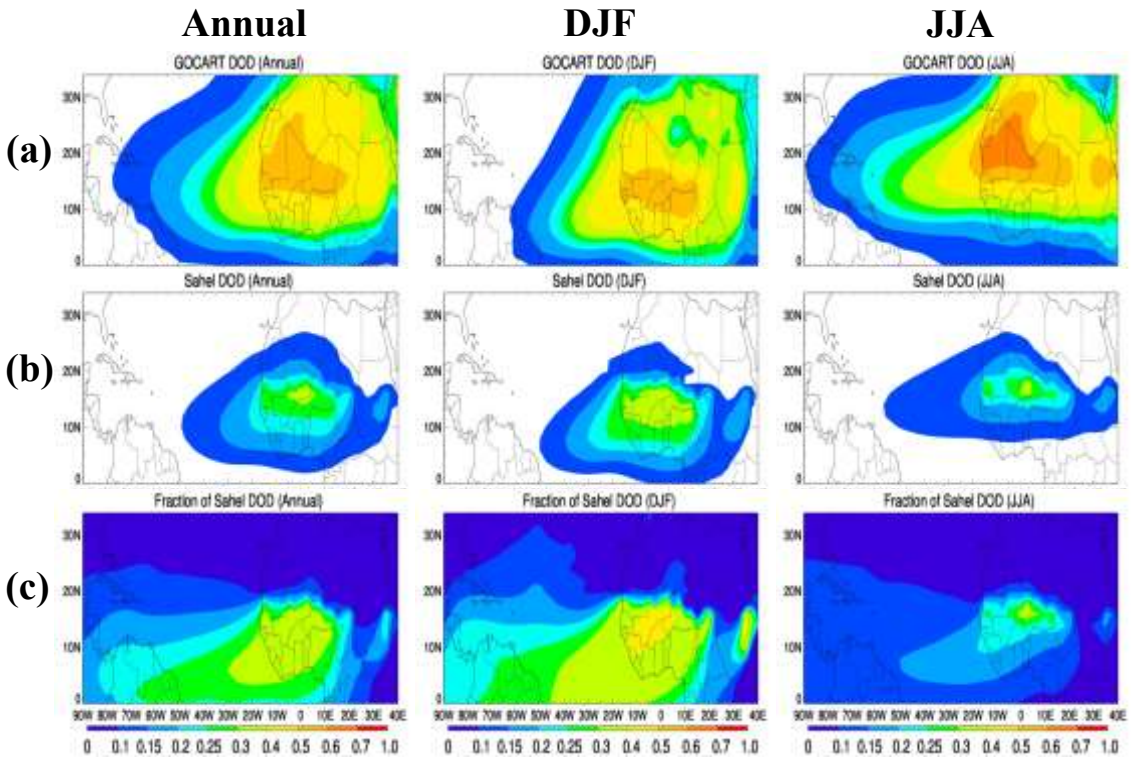

Figure 7. (a) Dust optical depth from GOCART base run averaged for 1982-2008, (b) dust optical depth from the Sahel, and (c) the ratio of the Sahel DOD to the base run for annual, winter, and summer.

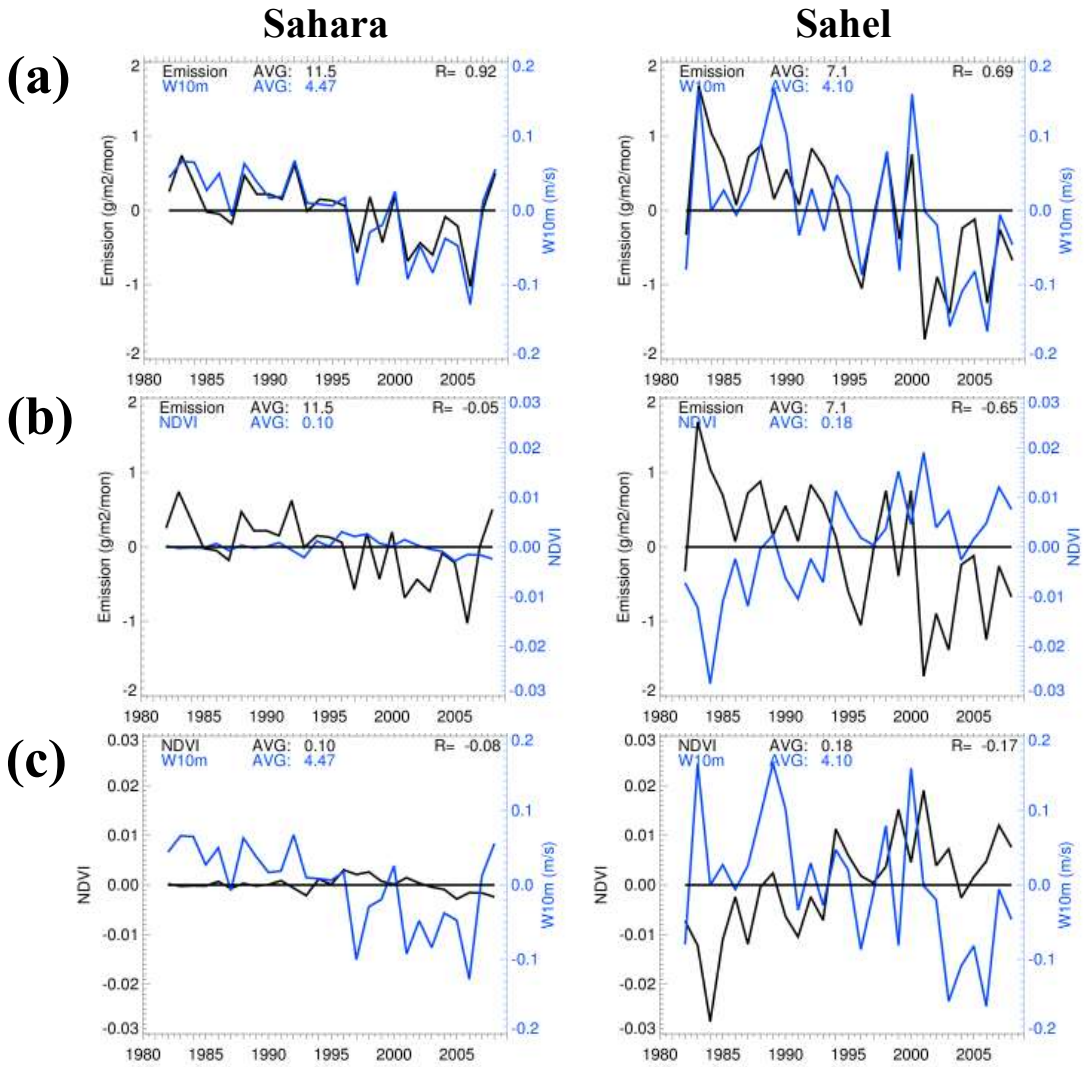

Figure 8. Time series of mean, anomalies, and correlation coefficients of (a) emission and W10m, (b) emission and NDVI, and (c) NDVI and W10m from 1982 to 2008 over the Sahara and Sahel.

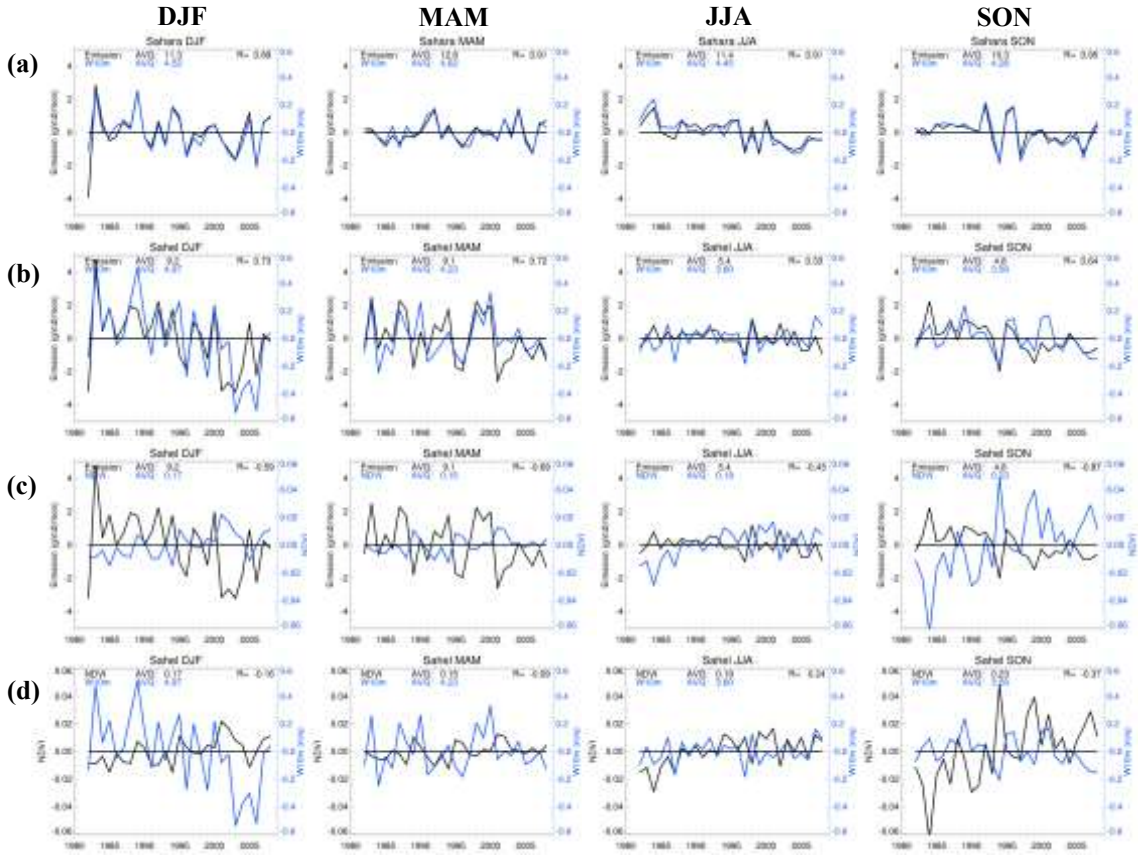

Figure 9. Time series of anomalies to seasonal mean over the Sahara (a) and Sahel (b-d) from 1982 to 2008 for each season: (a,b) emission and W10m, (c) emission and NDVI, and (d) NDVI and W10m. AVG and R refer to mean and correlation coefficient, respectively.

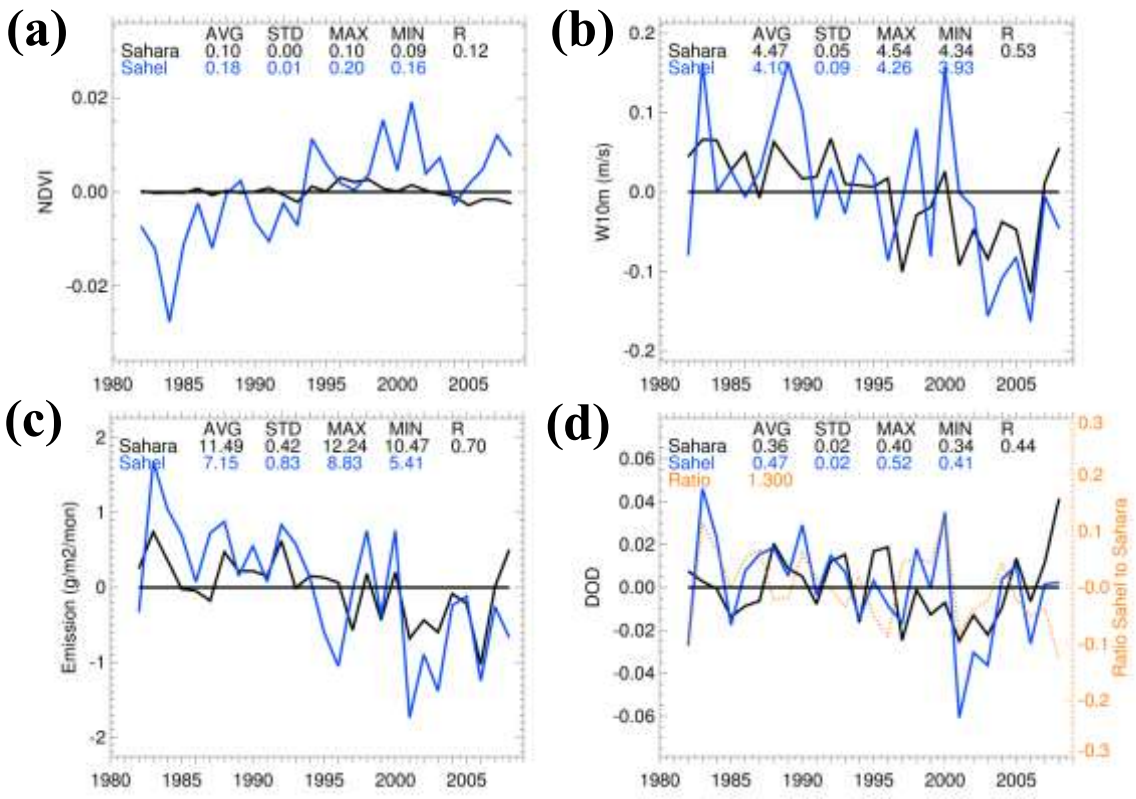

Figure 10. Time series of anomalies to mean over the Sahara and Sahel from 1982 to 2008 for (a) NDVI, (b) W10m, (c) emission, and (d) DOD. AVG, STD, MAX, MIN, and R refer to mean, standard deviation, maximum value, minimum value, and correlation coefficient between the Sahara and the Sahel, respectively.

Table 1. Correlation coefficients between variables over the Sahel averaged for 1982-2008. Parenthesis indicates the values over the Sahara. The asterisk symbol indicates that the values are insignificant at the 5% level.

	NDVI	W10m	Rainfall	EMI	LOAD
NDVI	1	-0.637	0.607	-0.872	-0.626
W10m	-	1	-0.823	0.897 (0.911)	-0.106* (0.132*)
Rainfall	-	-	1	-0.828	-0.075*
EMI	-	-	-	1	0.311* (0.308*)
LOAD	-	-	-	-	1